Wear 274–275 (2012) 238–247

Contents lists available at SciVerse ScienceDirect

Wear

journal homepage: www.elsevier.com/locate/wear

Scratching polycarbonate: A quantitative model

L.C.A. van Breemen[a,b,*], L.E. Govaert[a,b], H.E.H. Meijer[a,b]

[a] Polymer Technology, Eindhoven University of Technology, P.O. Box 513, NL-5600 MB Eindhoven, The Netherlands
[b] Dutch Polymer Institute (DPI), P.O. Box 902, NL-5600 AX, Eindhoven, The Netherlands

ARTICLE INFO

Article history:
Received 30 March 2011
Received in revised form 29 August 2011
Accepted 6 September 2011
Available online 17 September 2011

Keywords:
Contact mechanics
Single-asperity sliding friction
Polymer glasses
Intrinsic behavior
Scratch testing
Finite element modeling

ABSTRACT

Generally it is understood that friction is additively decomposed into an adhesion- and a deformation-related component, suggesting independence. Experimentally these components cannot be separated and only by combining experiments with simulations, a decoupled analysis is possible. We apply this hybrid experimental–numerical approach in the single-asperity scratch test, simplifying the friction geometry. Simulations without adhesive interaction between tip and surface result in friction forces that are only half of the experimental ones, and are almost not influenced by the sliding velocity. In case of an additive decomposition, this would imply a large contribution of the adhesive component which, moreover, should take care of all rate dependency. This sounds unrealistic. By inclusion of constant friction between tip and polymer, we find that the adhesive component strongly influences the contribution of the deformation component by the formation of a bow wave in front of the sliding tip. Experimental friction forces are quantitatively predicted, including the rate dependency. This entails that the suggested additive decomposition is not applicable and the large macroscopic deformation response proves to be the result of small changes in local processes. Using the model, for the first time, quantitative relations between the polymer's intrinsic mechanical properties and its frictional properties are established.

1. Introduction

Polymers display a unique strength-to-weight ratio and are, therefore, applied also in structural applications. In combination with their excellent tribological properties [1] they are moreover favored above their metal counterparts in applications where friction and wear are important, like e.g. in bearings and gears, and in hip-joints and artificial knees. However, tribology of polymers is still poorly understood and the relation between intrinsic polymer properties and frictional behavior is blurred, also because experiments usually have too many variables. Even in the case of single-asperity scratching, we find a dependence on scratch load, time, temperature, and speed, on the tip geometry [2–10], and the amount and type of fillers or additives [11–15].

The earliest model trying to predict the frictional response dates back to the pioneering work of Bowden and Tabor [16,17]. They presumed that the friction force can be additively decomposed into an adhesion- and a deformation-related component. Confirmation of this hypothesis was demonstrated by experiments on rubbers using rather specific boundary conditions, e.g. lubrication of the interface [18,19] or application of rolling friction [20,21]. With lubrication of the two contacting surfaces the adhesion component could be neglected and, as a result, the deformation related component was studied individually. To prevent a contribution of the lubricant in the shear layer, rolling friction was used, i.e. rolling a hard asperity over the rubber surface. Grosch [22], Ludema and Tabor [21], and Bueche and Flom [19] demonstrated by sliding at various velocities and temperatures on a given surface, that the frictional behavior of a rubber can be described by a single master curve, constructed by application of the WLF transform. Similar observations were reported by McLaren and Tabor [23] for polymers below their glass transition temperature. In the case of lubricated or rolling friction the comparison is most successful [24]. These observations indicate that capturing visco-elastic properties is of utmost importance.

To study mechanical properties of coatings, of thin films and on a small scale, usually indentation tests are performed, where a single-asperity contact (a well-defined indenter) is pressed into a substrate. In particular for the elastic modulus, based on a fully elastic response, quantitative analytical methods are available [25,26], and with the aid of the elastic-visco-elastic correspondence principle these methods can be applied to visco-elastic properties [27–31]. These approaches, in some sense, all assume an elastic response upon unloading, which is impossible to realize in a visco-elastic medium. Hence all attempts to improve on these methods will prove to be uphill battles. Less straightforward is the

* Corresponding author at: Polymer Technology, Eindhoven University of Technology, P.O. Box 513, NL-5600 MB, Eindhoven, The Netherlands.
Tel: +31 0 40 247 3092; fax: +31 0 40 244 7355.
E-mail address: l.c.a.v.breemen@tue.nl (L.C.A. van Breemen).
URL: http://www.mate.tue.nl/mate/showemp.php/4008 (L.C.A. van Breemen).

0043-1648/$ – see front matter © 2011 Elsevier B.V. All rights reserved.
doi:10.1016/j.wear.2011.09.002

analysis of the large strain mechanical properties, and e.g. for something trivial as the yield strength only empirical scaling laws are available [17,32–34].

For non-linear contact problems, the development of the Finite Element Method (FEM) opened up new possibilities. With appropriate finite-strain constitutive relations a detailed analysis of local deformation and stress fields became feasible. An example is the work in Larsson's group on Vickers [35] and Berkovich [36] indentation of elasto-plastic materials. For polymers, the analysis of such a contact problem is more complex. Crucial proves to be the application of a quantitative constitutive model that properly captures the intrinsic polymer properties [37–39].

The next challenge, after successfully modeling the indentation test, is the evaluation of the single-asperity sliding friction test. This test is commonly referred to as a scratch test and is extensively used to determine a wide range of surface mechanical properties, like the relative hardness of materials and in the modeling of wear [40–43]. The friction (and wear) behavior of polycarbonate (PC) has been subject of study [3,5,6,43], however mostly experimental. Similar to indentation, the FEM technique has been employed to analyze the complex material response as observed in scratch experiments [44–47]. The group of Schirrer [48–52] recently tried to quantify experimental data on polymethylmethacrylaat (PMMA). The experimental set-up developed allows the in situ determination of the real contact area [53]. The problem is analyzed quasi-statically, which implies that there is no time-dependence and thus no dependence on strain rate or sliding velocity; this is a strong assumption. The constitutive relation employed does not capture the large strain mechanics, and neither correctly captures the visco-elastic pre-yield behavior of polymer glasses. Despite these obvious drawbacks a qualitative relation between contact area and simulated friction coefficient could be established. An analogous approach by Bucaille et al. [45], employing the same constitutive relation, shows that a relation between strain hardening and observed frictional hardness can be achieved. Still, as also pointed out by Briscoe and Sinha [54], at present, there are no analytical or computational models available to quantitatively couple intrinsic material properties to the observed frictional response. Therefore there is a need for an appropriate finite-strain constitutive relation that accurately captures these intrinsic deformation characteristics.

In this study, FEM analyses are employed to investigate the role of the interaction between indenter and polymer on the friction force, using the EGP-model [55] that captures the small and large strain intrinsic mechanical response of polymer glasses in a quantitative way. The choice for glassy polymers is therefore not motivated by their relevance for low friction applications, but they can serve as model systems because they represent the best characterized class of polymers that allows quantitative predictions, also in contact mechanics. Using FEM modeling combined with well-defined experiments, the interaction between tip and polymer can be separately studied. The challenge in the experiments is to perform reproducible sliding friction tests with a minimum number of variables.

The intrinsic pre-yield regime of polymers is non-linear visco-elastic and correct modeling thereof is important in all simulations where, during loading and unloading, non-homogeneous deformations result, like e.g. in indentation or sliding friction tests. The original EGP-model uses one mode only, and thus behaves as a compressible linear elastic solid. As a result, details of the indentation test were not quantitatively described. Including a spectrum of relaxation times using a multi-mode approach solved this problem [56,57]. The model was quantitative while its only adjustable parameter is the one that represents the thermodynamic state of the material. However, as demonstrated by Engels et al. [58,59] once the details of the formation history of the polymer product are known, this state can directly be computed.

We will use the multi-mode version of the EGP-model to compute the complex single-asperity sliding friction test. By comparing simulations with experiments we can isolate the individual influences, like deformation and adhesion, on the friction force and investigate the precise influence of the polymer's intrinsic mechanical behavior.

2. Experimental

2.1. Sample preparation

The material used is a commercial grade of polycarbonate, Lexan 101R, Sabic Innovative Plastics (Bergen op Zoom, The Netherlands).

The scratch samples are prepared from compression molded plaques (50 mm × 50 mm × 10 mm). During compression molding the dried granulate is heated in a mold for 15 min at 250 °C and next compressed up to 300 kN in five subsequent intervals of 5 min, while after each step degassing is allowed by releasing the force. Finally the mold is placed in a water-cooled cold press and quenched to room temperature (20 °C) under a moderate force of 100 kN.

The mean surface roughness (R_m) of the plaques is in the order of 10 μm, which is of the same order as the tip-radius in the scratch set-up. To consider the surface of the polymer sample flat, as compared to the indenter tip, we need samples with a roughness, R_m, of at most 50 nm which is realized by compressing the samples against an optically flat steel plate ($R_m \approx 5$ nm). Thereto, the samples are placed on a preheated (190 °C) optically flat steel plate and placed in an oven for 30 min at 190 °C, since this is approximately 40 °C above the T_g of PC, the now rubbery PC-sample is subsequently placed in a hot-press (200 °C) and compressed with a force of 300 kN for 15 min; thereafter it is transfered to the cold press. To obtain samples with a uniform thickness of 3 mm, spacers are placed alongside the steel plate during these compression steps. The compression procedure introduces stresses in the surface layer, where the single-asperity scratch tests are performed. Because experiments are compared to simulations, where uniform material properties and stress-free initial conditions are assumed, removal of frozen-in stress and orientations is essential. Thereto the samples are placed in the oven once more at 190 °C for 30 min, and subsequently air-cooled to room temperature. The surface roughness is checked with a profilometer (Sensofar®) and proved to be $R_m \approx 20$ nm (see Fig. 1).

2.2. Techniques

Single-asperity scratch experiments are performed using a standard nano-indenter XP (MTS Nano-Instruments, Oak Ridge, Tennessee) extended with the lateral force option. The normal load applied is force controlled, whereas the sliding velocity is under displacement control. The two round-tip geometries used (see Fig. 2) are characterized by the Sensofar and by SEM and both have a top angle (α) of 90° and different top-radii (r_{tip}), 10 μm and 50 μm respectively. To accomplish a perfect perpendicular position of the tip versus the sample surface and arrive at a parallel sliding path, a specially designed alignment tool is employed. Details on the alignment tool can be found elsewhere [60].

2.3. Choice of tip geometry

The nano-indenter can be equipped with different indenter tips. The Berkovich tip has sharp edges that result in complex deformation fields underneath the indenter tip; therefore this tip is not the obvious choice. The cone-shaped indenter has only one parameter, the top angle (α), but from a FEM point of view also this tip is not the evident choice since convergence problems are anticipated

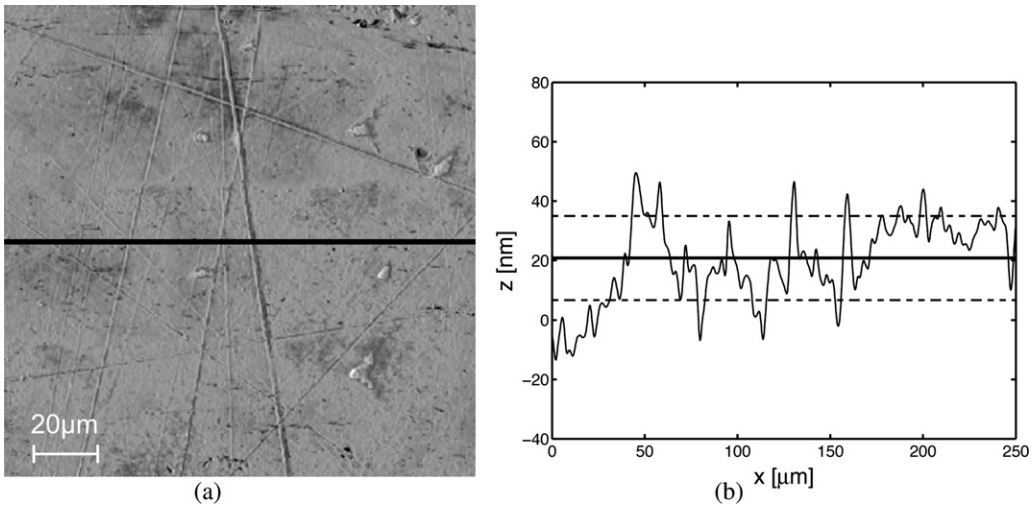

Fig. 1. (a) Surface profile obtained from the Sensofar profilometer; the solid line (–) is the location where the mean surface roughness is determined; (b) surface roughness of the Lexan 101R sample, where the horizontal solid line (–) is the mean surface $R_m \approx 20$ nm and the dashed lines (- -) are the corresponding standard deviations.

around the sharp indenter tip, leading to singularities. Therefore we choose for the round tip, characterized by its top angle α and top radius r_{tip}. This tip does not induce singularities since the mesh can 'flow' underneath the tip. Moreover no sharp edges are present, therefore less pronounced mesh refinements are needed and far better convergence results due to smaller local gradients.

2.4. Effect of sample tilt

Misalignment is defined as the situation where the sample surface is not perpendicular to the symmetry axis of the indenter tip. Two types of misalignment exist, the first is between sample and tip, the second between machine and tip, where wrong mounting results in off-axis loading. Presuming that the tip is well-mounted, only the first misalignment option remains. Fig. 3 illustrates its (exaggerated) effect resulting in completely different deformation responses.

To prevent this, the home-made alignment tool is utilized (see Fig. 4) but because the nano-indenter XP is extended with the lateral force option, and as a result in-plane movement is possible, a different, simple and less time-consuming, alignment procedure can be applied as compared to the one described in Pelletier et al. [60] for flat-tip indentation.

They had to measure the contact stiffness, which is maximum when tip and sample are correctly aligned, and this requires an elaborate test procedure. We simply mount the sample in the alignment tool, which is set in neutral position, and make two initial perpendicular scratches, parallel to each of the rotation axes of the device (length 1 mm, normal load 50 μN, sliding velocity 10 μm s^{-1}). The sample tilt is determined from the raw signal that gives the displacement into the surface. Next the sample rotation required is calculated via elementary goniometric relations and applied accordingly. Completion of this procedure on both rotation axis leaves a perfectly aligned sample–tip combination.

2.5. Dependence on sliding velocity

Parameters in the scratch test are, apart from temperature, humidity and the geometry of the indenter tip, the normal load (F_n), and the sliding velocity (v) applied. Both can be chosen constant, or increasing or decreasing. Differences in the deformed material volume result. The penetration into the surface (Δy) and the lateral force (F_f) are measured (see Fig. 5). To avoid complex interactions, inert diamond round tips, 50 μm and 10 μm, are selected.

Sliding velocity and temperature are taken constant in each experiment, as well as the normal force. At the start of an experiment, the load is applied in 10 s, without sliding, which is in principle a normal indentation [39,56,57].

Fig. 6 illustrates the typical response observed when the described loading protocol is executed. The lines are the average of five consecutive measurements with identical input parameters.

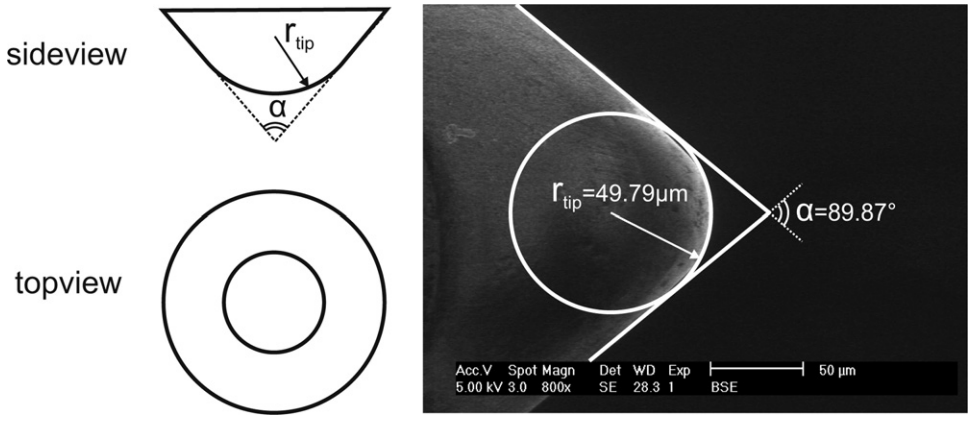

Fig. 2. Characterization of the used 50 μm round tip by SEM, here α is the top angle and r_{tip} the radius of the tip.

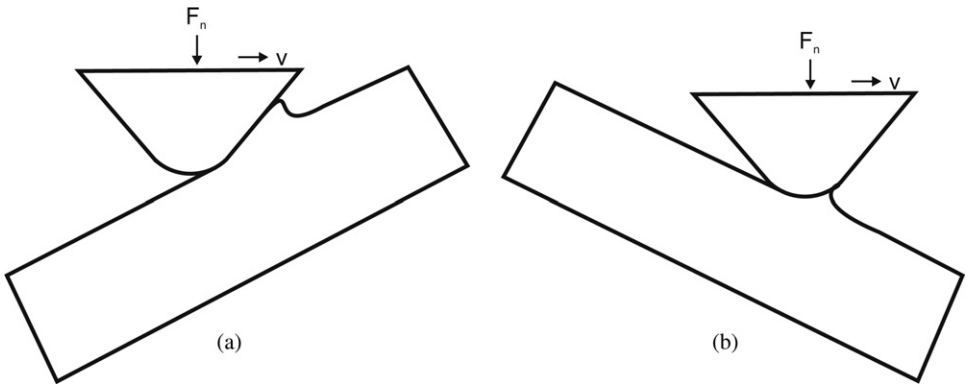

Fig. 3. Exaggerated effect of sample–tip misalignment, resulting in different deformation responses.

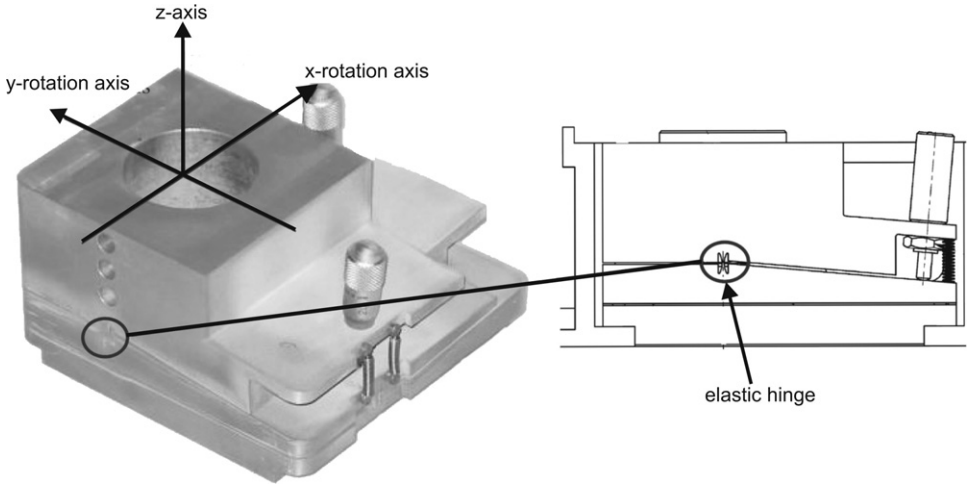

Fig. 4. Sample-tilt stage based on elastic hinges developed at the TU/e [60].

Fig. 6(a) shows the penetration into the surface as a function of scratch distance, and Fig. 6(b) gives the lateral force. Three points are indicated, marked I, II, and III, and visual impressions sketched are in Fig. 6(c). Indentation (I) results in an indentation depth marked by the dashed line. Next we start sliding (I–II) to notice that (in this force controlled experiment) the contact surface generated during indentation is reduced, resulting in sink-in of the tip into the polymer (II). After point III, a steady state is reached and a bow wave has developed in front of the tip. The new contact area generated remains constant during the remainder of the sliding test. Only steady state data are used in the analyses.

Results of four experiments, differing only in sliding velocity, ranging over four decades from 0.1 $\mu m\,s^{-1}$ to 100 $\mu m\,s^{-1}$, are shown in Fig. 7.

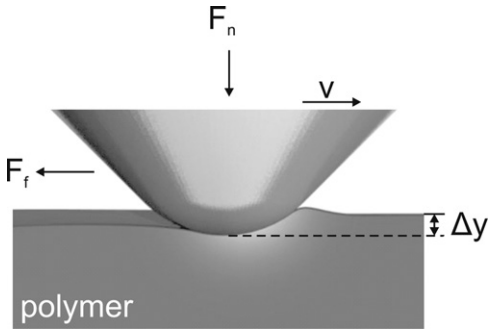

Fig. 5. The single-asperity scratch set-up with characteristic in- and output parameters.

Both penetration depth into the surface and lateral force display a clear dependency on sliding velocity. The rationale is given by the fact that polymers intrinsically display a pronounced strain-rate dependence, and thus a dependence on sliding velocity is expected. With increasing velocity the material displays more resistance to deformation and, as a consequence, the tip penetrates less into the surface (Fig. 7(a)). A decrease in contact area between tip and polymer results, and the lateral force, which is directly related to this contact area, therefore also decreases (Fig. 7(b)).

Since the yield stress of polymers linearly depends on the logarithm of the strain rate [55], we plot the measured lateral force versus the logarithm of sliding velocity applied (see Fig. 8). A linear relation is found.

3. Modeling

3.1. Constitutive model

The constitutive model employed [55–57] is implemented in the FEM package MSC.Marc and it is based on an additive decomposition of the total stress into a driving and a hardening stress. The hardening stress is modeled with a neo-Hookean spring and accounts for the stress contribution of the orienting entangled molecular network. The driving stress is additively decomposed into a hydrostatic and deviatoric part and is related to the intermolecular interactions. The deviatoric part ($\boldsymbol{\sigma}_s^d$) is coupled to the plastic deformation rate tensor ($\mathbf{D}_p$) via a non-Newtonian flow rule. The viscosity depends strongly on equivalent stress ($\overline{\tau}$),

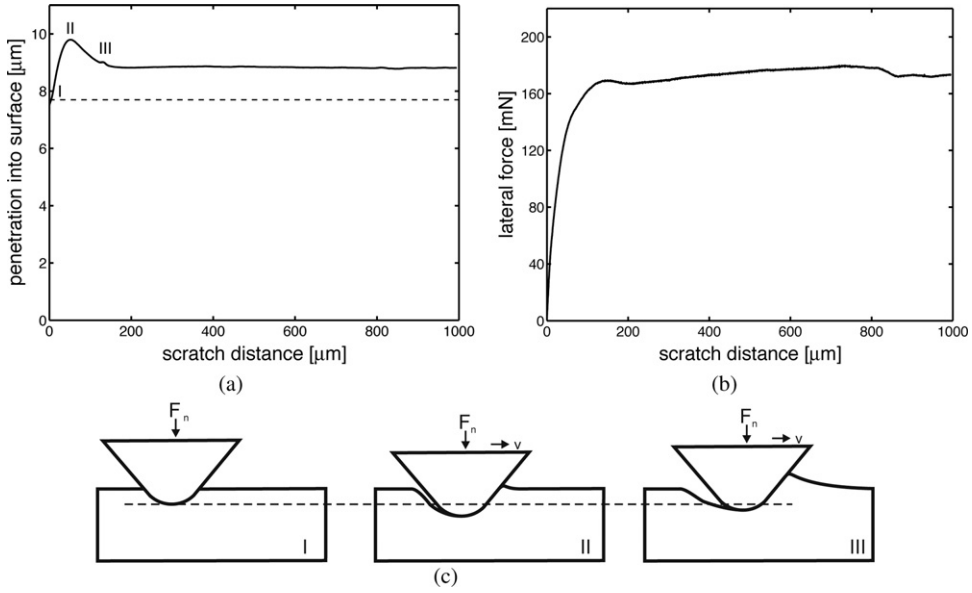

Fig. 6. Measured response of a single-asperity scratch experiment with a constant normal load of 300 mN and a sliding velocity of 0.1 μm s^{-1}; (a) penetration into the surface versus sliding distance, (b) the lateral friction force versus sliding distance and (c) graphical representation of the observed macroscopic response; the numbers I, II, and III, correspond to the same numbers as in (a), where the dashed line (- -) is the depth after the initial indentation step.

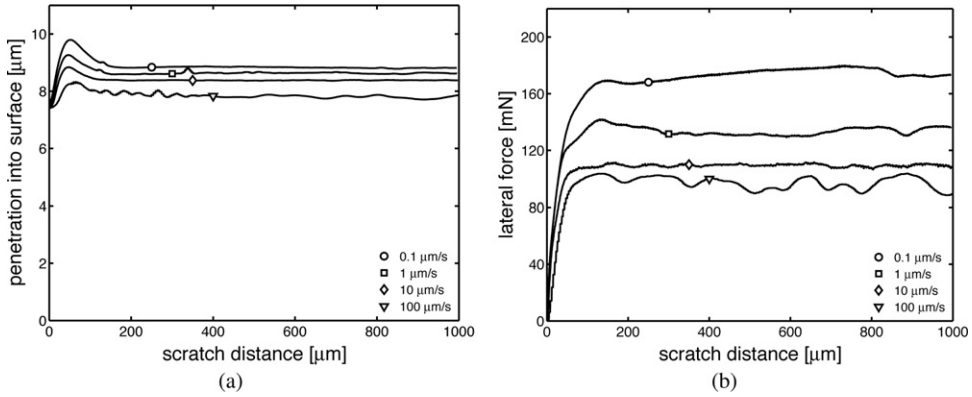

Fig. 7. Response of Lexan 101R at four different sliding velocities with a 50 μm tip; (a) penetration into the surface versus sliding distance and (b) friction force versus sliding distance.

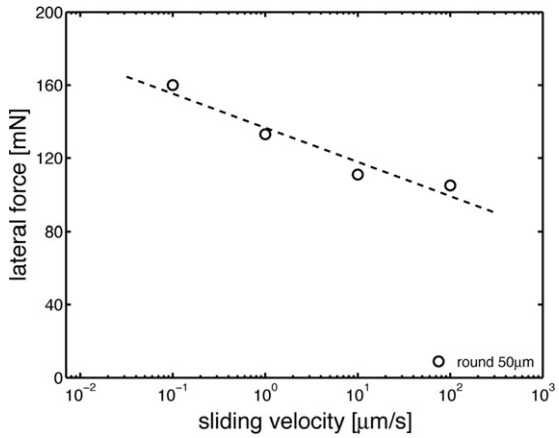

Fig. 8. Response of Lexan 101R at four different sliding velocities; friction force versus logarithm of sliding velocity, the dashed line (- -) is a first order fit of the experimental data and plotted as a guide to the eye.

temperature (T), hydrostatic pressure (p) and thermodynamic state (S_a) of the material, according to:

$$\mathbf{D}_{p,i} = \frac{\boldsymbol{\sigma}_s^d}{2\eta_i(\overline{\tau}, T, p, S_a)},$$

$$\text{where} \quad \eta_i = \eta_{0,i,\text{ref}}(T)\frac{\overline{\tau}/\tau_0(T)}{\sin h\left[\overline{\tau}/\tau_0(T)\right]} \exp\left[\frac{\mu p}{\tau_0(T)}\right] \exp\left[S_a R(\overline{\gamma}_p)\right]. \tag{1}$$

The only unknown parameter in the model is the parameter capturing the present thermodynamic state of the material (S_a). It has been shown that its value can directly be determined from an indentation test, by matching the load-displacement response to the simulation [39]. Since every sliding friction experiment starts with an initial indentation, the value of S_a is easily determined.

3.2. Finite element mesh

Since the problem analyzed is symmetric in sliding direction, only half the scratch surface is meshed. The mesh for the 50 μm tip consists of 33904 linear brick elements (hex 8,

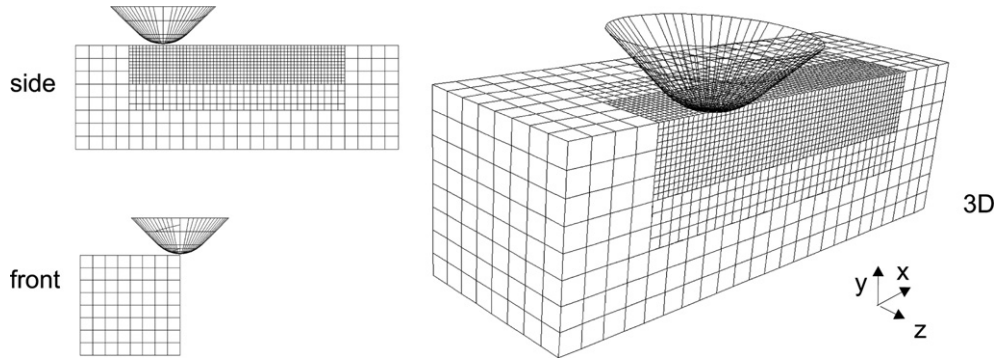

Fig. 9. Mesh for the 50 μm tip.

element number 7, full integration) (see Fig. 9), with dimensions 0.16 mm × 0.16 mm × 0.48 mm, such that the edges have no influence on the stress-field. Usually when large deformations are expected, quadratic elements are preferred (no locking), however, in contact analyses linear elements are recommended, [61]. The tip geometry is an exact copy of the surface profile generated by the Sensofar, and is modeled as a rigid impenetrable surface. The contact between indenter and polymer is initially assumed to be frictionless, because only the deformation related component is studied. Later, Coulomb friction is added to the simulations to study the effect of polymer–tip interaction.

3.2.1. Boundary conditions

Front, back, sides, and bottom are restrained in all directions. The symmetry plane is fixed only in *z*-direction. The behavior of the indenter is prescribed by a reference node on the surface. Throughout the simulation, the displacement of the reference node in *z*-direction is fixed and the chosen sliding velocity in *x*-direction is applied. Since only half the scratch surface is meshed, the normal load F_n applied is therefore also divided by two, resulting in 150 mN. The simulation is split in two parts, first indentation with 150 mN in 10 s, thereafter sliding with constant velocity and normal load.

3.2.2. Mesh refinement

To keep complete connectivity between all neighboring elements, mesh refinement is needed of e.g. a factor two in all directions, increasing the number of hexagonal elements with a factor eight. Calculation times in 3D scale at least linearly with the number of elements, and at most with the number of elements squared, resulting in an 8–64 increase in time. Therefore only regions of interest are refined (see Fig. 9). To attach discontinuous element-edges the glue option is used, which results in an extra contact constraint in the contact table. In Fig. 10 the different contact bodies are depicted with different gray-values. Despite all these efforts, a simulation takes, on 16 parallel CPU's (1.8 GHz AMD Opteron with 32GB RAM), approximately one week.

3.3. Influence of sliding velocity without friction

Indentation can be considered completely frictionless [39], and even when a friction model is added, the value of S_a will not change. The state parameter is uniquely defined, resulting in $S_a = 25.1$ for our samples. Now frictionless scratching at different sliding velocities is simulated (see Fig. 11), calculating only the deformation related contribution.

When the friction force is additive in deformation and adhesion [62], the last component should cover for the difference between the solid and the dashed line, which implies that adhesion should not only give rise to almost half of the friction force, but also should be responsible for almost all the rate (velocity) dependency. This sounds weird and rather unphysical.

3.4. Influence of sliding velocity with friction

Friction is a complex physical phenomenon involving surface roughness, temperature, contact stresses and relative velocities. In the FEM package MSC.Marc, several friction models are available varying from the most simple, and thus most popular, friction model, which is Coulomb friction, to the more complex bilinear models. With increasing complexity also the number of

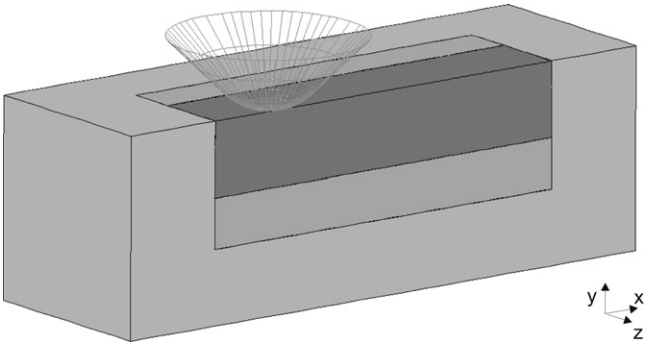

Fig. 10. The different gray-values indicate the different contact bodies defined.

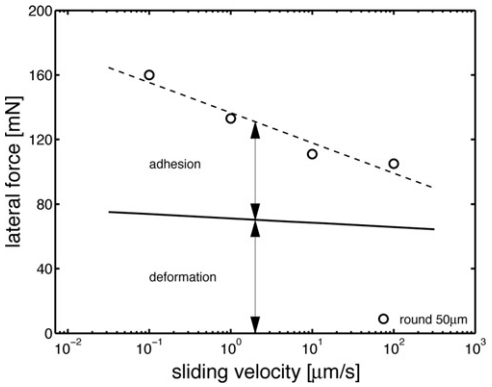

Fig. 11. Simulations of sliding friction experiments result in the solid line (–), where the fitted experimental data are depicted with the dashed line (--); the difference results in the additive decomposition of the measured friction force into a deformation and an adhesion component.

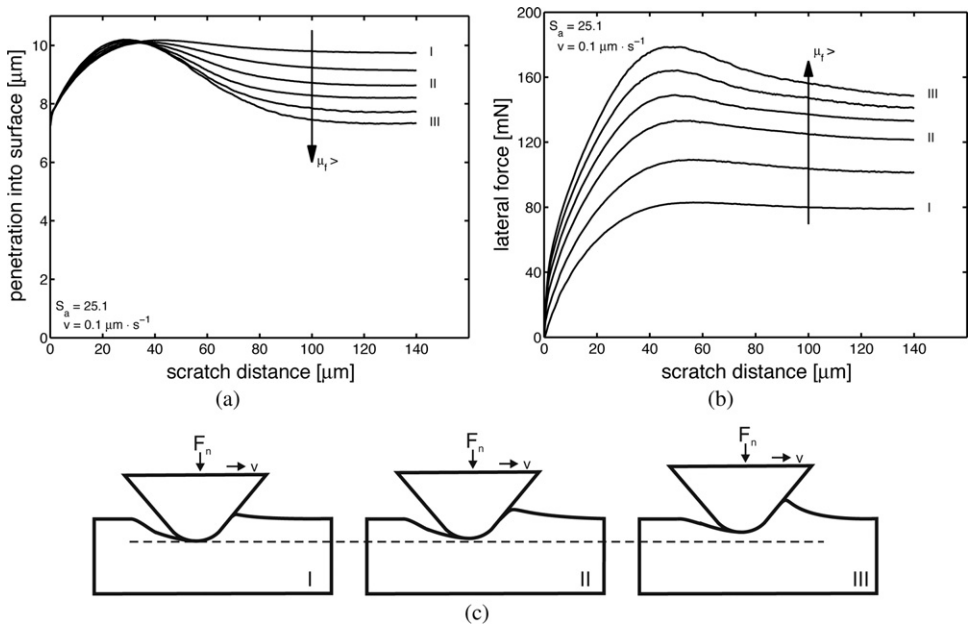

Fig. 12. Simulated response of a single-asperity scratch experiment with a constant normal load of 300 mN and a sliding velocity of 0.1 μm s^{-1}, with μ_f ranging from 0.0 to 0.2; (a) penetration into the surface versus sliding distance, (b) the lateral force friction versus sliding distance and (c) graphical representation of the observed macroscopic response; the numbers I, II, and III, correspond to the same numbers as in (a) and (b), where the dashed line (- -) is the depth when sliding with $\mu_f = 0.0$.

friction-model input parameters increases drastically and, as a consequence, data interpretation becomes blurred by the amount of variables used. Our choice for the Coulomb model is obvious, concerning the prior mentioned arguments. Please note in this respect that the Coulomb friction model is velocity (rate) independent. The model is given by:

$$\|\vec{f}_t\| = \mu_f f_n \quad \text{(stick) and} \quad \vec{f}_t = -\mu_f f_n \vec{t} \quad \text{(slip)} \tag{2}$$

where $\vec{f}_t$ is the tangential (friction) force, f_n is the normal force, μ_f is the (constant) local friction coefficient and $\vec{t}$ the tangential vector in the direction of the relative velocity, defined according to:

$$\vec{t} = \frac{\vec{v}_r}{\|\vec{v}_r\|}, \tag{3}$$

in which $\vec{v}_r$ is the relative sliding velocity. For a given normal force, f_n, the friction force shows a step function, based on the value of the

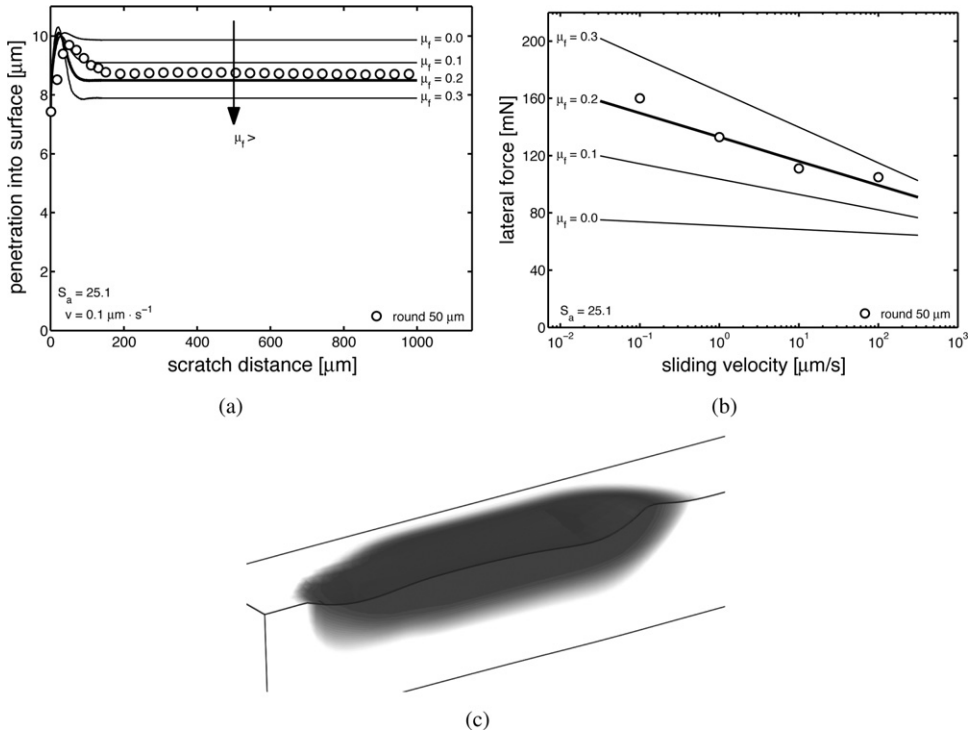

Fig. 13. (a) Simulated penetration into the surface for different values of μ_f at a sliding velocity of 0.1 μm s^{-1} compared to experimental data; (b) friction force versus the logarithm of sliding velocity compared to simulations with different values for μ_f; (c) simulation of the plastic deformation zone, where black is visco-plastic deformation and white is undeformed or visco-elastic deformation.

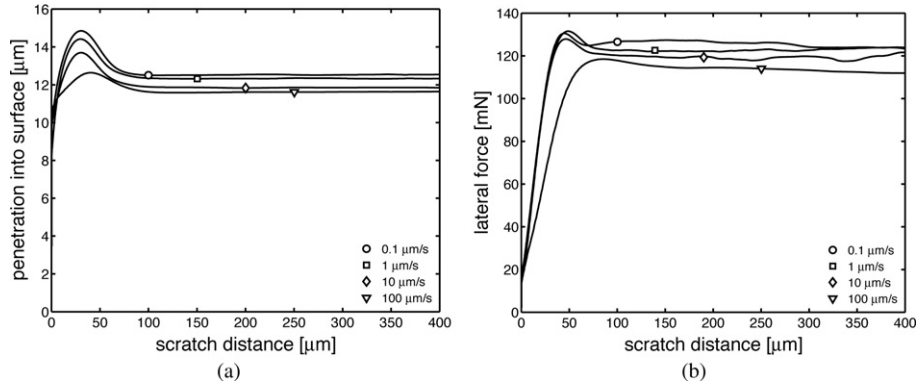

Fig. 14. Response of Lexan 101R at four different sliding velocities with a 10 μm tip; (a) penetration into the surface versus sliding distance and (b) friction force versus sliding distance.

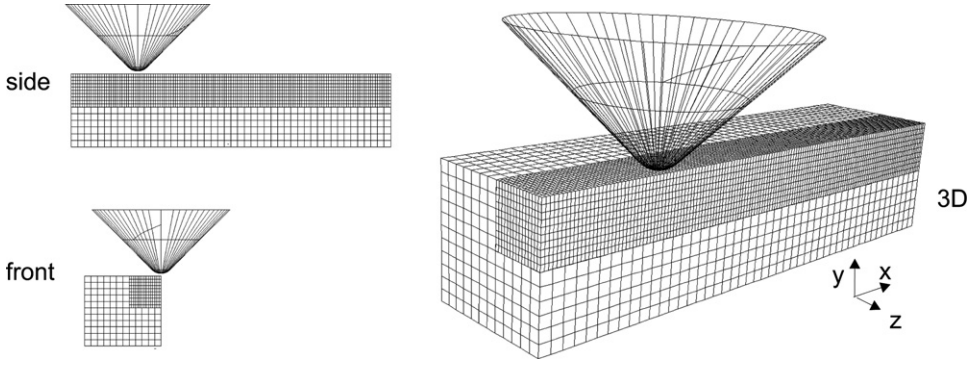

Fig. 15. Mesh for the 10 μm tip.

relative sliding velocity $\vec{v}_r$. Since this discontinuity in friction value causes numerical difficulties, different approximations of this step function are available, the most basic one using an arctangent. Since other approximations introduce more model parameters, they are discarded here. The arctangent model reads:

$$\vec{f}_t = -\mu_f f_n \frac{2}{\pi} \arctan\left[\frac{\|\vec{v}_r\|}{\delta}\right] \vec{t}. \tag{4}$$

Physically, δ is interpreted as the value of the relative velocity below which sticking occurs. Typically, a value of 1–5% of the applied sliding velocity gives realistic simulation data [63].

For a sliding velocity of 0.1 μm s^{-1} the effect of adding friction, is shown in Fig. 12, plotting the penetration into the surface and the corresponding lateral force. A huge increase in lateral force results (Fig. 12(a)), which is not caused by a sink-in of the tip, that clearly penetrates less into the surface (Fig. 12(a)), but by the formation of a bow wave in front of the sliding tip (Fig. 12(c)). The formation of the

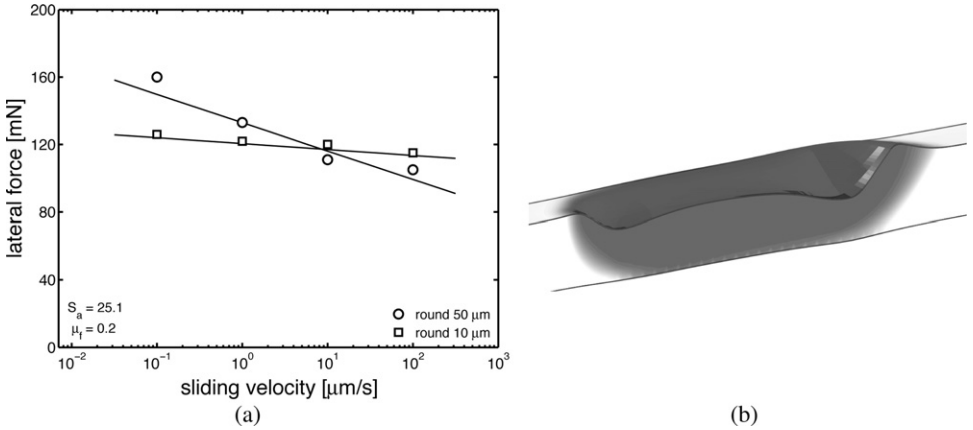

Fig. 16. (a) Friction force versus the logarithm of sliding velocity, where the experimental data of the sharp 10 μm tip (□) and the blunt 50 μm tip (○) are compared to simulations with identical thermodynamic state of the material (S_a = 25.1) and a similar local friction coefficient (μ_f = 0.2); (b) simulation of the plastic deformation zone, where black is visco-plastic deformation and white is undeformed or visco-elastic deformation.

bow wave mainly results from the increase in frictional shear stress along the contact surface. To obtain a representative value of the friction coefficient by comparing simulations with experiments, a value of $\mu_f = 0.2$ results (see Fig. 13).

We can conclude that a quantitative comparison between simulations and experiments is possible. However, confirmation requires an independent validation experiment with corresponding simulations. Therefore the tip geometry is changed.

3.5. Influence of tip geometry

Experiments on the same material are performed, thus with an identical thermodynamic state, using a different indenter tip with radius of 10 μm. Being sharper, the tip will penetrate further into the surface, and therefore the normal load applied is reduced from 300 mN to 150 mN to obtain comparable penetrations. The experimental data are shown in Fig. 14. Because, when plotted over the total scratch distance of 1 mm, the data almost coincide to one curve, they are only shown up to a scratch distance of 0.4 mm.

The effect of the sliding velocity is much less pronounced when compared to the experiments performed with the 50 μm tip (see Fig. 7).

Next we simulate the experiments. The mesh used is shown in Fig. 15 and consists of 38,736 elements.

Identical boundary conditions as for the 50 μm tip mesh are applied, with this difference that the normal load is 75 mN instead of 150 mN. The local friction coefficient, $\mu_f = 0.2$, and thermodynamic state of the material, $S_a = 25.1$, are identical to the 50 μm tip simulations where a quantitative comparison was achieved.

All results are summarized in Fig. 16(a). Interestingly, also for the sharp tip quantitative predictions are made, including the (now only small) effect of the sliding velocity. Thinking about the bow wave effect for the blunted tip, this can be rationalized: one does not water ski on sharp skis.

4. Conclusions

Comparing numerical simulations with experimental results shows that quantitative predictions for the single-asperity sliding friction tests indeed are possible. The best value for the friction coefficient between indenter and polymer is $\mu_f = 0.2$, but a much more important conclusion is that friction between diamond indenter and polymer only indirectly contributes to the lateral (friction) force, via an increase of the plastic deformation zone. Simulations with no adhesive interaction between tip and polymer yield only half of the experimental lateral (friction) force and, moreover, show almost no influence of the sliding velocity, the solid line for $\mu_f = 0.0$ in Fig. 11, whereas experiments show a significant influence. In case of an additive decomposition, this would imply not only a huge contribution of adhesion, but also a rate/velocity-dependency of the adhesive component. By including the velocity (rate) independent Amontons–Coulomb friction law, which creates an interaction between tip and polymer, the suggested additive decomposition is proved not to be applicable and the large macroscopic deformation response proves to be the result of small changes in local processes. When indenter–polymer interaction is taken into account, a bow wave is formed in front of the sliding tip, which leads to an increase in contact area between tip and polymer and results in an increase in friction force. The experimentally observed time-dependent behavior of the friction force can solely be attributed to the polymer's intrinsic deformation response. The same holds for the dependence of friction force on sliding velocity. Also that can be solely attributed to the influence of strain rate on the intrinsic properties of the polymer investigated. The quantitative capability of the modeling framework is confirmed by performing simulations on the same material, thus identical thermodynamic state (S_a) and friction coefficient (μ_f), but with a different tip geometry and normal load applied, resulting in an accurate prediction of the friction force measured. Remarkable is that in both the simulations and the experiments the so-called velocity-weakening, the decrease in friction force with increasing sliding velocity, is strongly indenter geometry dependent; since its geometry directly sets the plastic deformation zone.

References

[1] S.W. Zhang, State-of-the-art of polymer tribology, Tribol. Int. 31 (1–3) (1998) 49–60.
[2] B.J. Briscoe, K.S. Sebastian, The elastoplastic response of poly(methyl methacrylate) to indentation, Proc. R. Soc. Lond. A 452 (1996) 439–457.
[3] B.J. Briscoe, E. Pelillo, S.K. Sinha, Scratch hardness and deformation maps for polycarbonate and polyethylene, Polym. Eng. Sci. 36 (24) (1996) 2996–3005.
[4] B.J. Briscoe, P.D. Evans, S.K. Biswas, S.K. Sinha, The hardnesses of poly(methylmethacrylate), Tribol. Int. 29 (2) (1996) 93–104.
[5] B.J. Briscoe, P.D. Evans, E. Pelillo, S.K. Sinha, Scratching maps for polymers, Wear 200 (1–2) (1996) 137–147.
[6] B.J. Briscoe, Isolated contact stress deformations of polymers: the basis for interpreting polymer tribology, Tribol. Int. 31 (1–3) (1998) 121–126.
[7] C. Xiang, H.-J. Sue, J. Chu, B. Coleman, Scratch behavior and material property relationship in polymers., J. Polym. Sci., Part B: Polym. Phys. 39 (1) (2001) 47–59.
[8] T. Baumberger, P. Berthoud, C. Caroli, Physical analysis of the state- and rate-dependent friction law. II. Dynamic friction, Phys. Rev. B 60 (6) (1999) 3928–3939.
[9] P. Berthoud, T. Baumberger, C. G'Sell, J.-M. Hiver, Physical analysis of the state- and rate-dependent friction law: static friction, Phys. Rev. B: Condens. Matter Mater. Phys. 59 (22) (1999) 14313–14327.
[10] J.A. Williams, Analytical models of scratch hardness, Tribol. Int. 29 (8) (1996) 675–694.
[11] R.S. Kody, D.C. Martin, Quantitative characterization of surface deformation in polymer composites using digital image analysis, Polym. Eng. Sci. 36 (2) (1996) 298–304.
[12] J. Chu, L. Rumao, B. Coleman, Scratch and mar resistance of filled polypropylene materials, Polym. Eng. Sci. 38 (11) (1998) 1906–1914.
[13] J. Chu, C. Xiang, H.-J. Sue, R.D. Hollis, Scratch resistance of mineral-filled polypropylene materials, Polym. Eng. Sci. 40 (4) (2000) 944–955.
[14] T. Goda, K. Varadi, K. Friedrich, H. Giertzsch, Finite element analysis of a polymer composite subjected to a sliding steel asperity: Part I – normal fibre orientation, J. Mater. Sci. 37 (8) (2002) 1575–1583.
[15] K. Friedrich, K. Varadi, T. Goda, H. Giertzsch, Finite element analysis of a polymer composite subjected to a sliding steel asperity Part II: parallel and anti-parallel fibre orientations, J. Mater. Sci. 37 (16) (2002) 3497–3507.
[16] F.P. Bowden, D. Tabor, The Friction and Lubrication of Solids, Oxford University Press, 2001.
[17] D. Tabor, Hardness of Metals, Clarendon Press, Oxford, 1951.
[18] J.A. Greenwood, D. Tabor, The friction of hard sliders on lubricated rubber: the importance of deformation losses, Proc. Phys. Soc. 71 (6) (1958) 989–1001.
[19] A.M. Bueche, D.G. Flom, Surface friction and dynamic mechanical properties of polymers, Wear 2 (3) (1959) 168–182.
[20] D. Tabor, The mechanism of rolling friction, Philos. Mag. 43 (345) (1952) 1055–1059.
[21] K.C. Ludema, D. Tabor, The friction and visco-elastic properties of polymeric solids, Wear 9 (5) (1966) 329–348.
[22] K.A. Grosch, Visco-elastic properties and the friction of solids: Relation between the friction and visco-elastic properties of rubber, Nature 197 (4870) (1963) 858–859.
[23] K.G. McLaren, D. Tabor, Visco-elastic properties and the friction of solids: friction of polymers: influence of speed and temperature, Nature 197 (4870) (1963) 856–858.
[24] B.J. Briscoe, D. Tabor, Friction and wear of polymers: The role of mechanical properties, Br. Polym. J. 10 (1) (1978) 74–78.
[25] H. Hertz, Uber die berhrung fester elasticher korper (on the contact of elastic solids), J. Reine Angew. Math. 92 (1881) 156–171.
[26] W.C. Oliver, G.M. Pharr, An improved technique for determining hardness and elastic-modulus using load and displacement sensing indentation experiments, J. Mater. Res. 7 (6) (1992) 1564–1583.
[27] L. Cheng, X. Xia, W. Yu, L.E. Scriven, W.W. Gerberich, Flat punch indentation of viscoelastic material, J. Polym. Sci. Part B 38 (1) (2000) 10–22.
[28] L. Cheng, X. Xia, L.E. Scriven, W.W. Gerberich, Spherical-tip indentation of viscoelastic material, Mech. Mater. 37 (2005) 213–226.
[29] J.M.J. den Toonder, Y. Ramone, A.R. van Dijken, J.G.J. Beijer, G.Q. Zhang, Viscoelastic characterization of low-dielectric-constant silk films using nano-indentation, in: Proceedings of the 3rd International Conference on Benefiting from Thermal and Mechanical Simulation in (Micro)-Electronics, 2002, pp. 270–280.
[30] J.M.J. den Toonder, Y. Ramone, A.R. van Dijken, J.G.J. Beijer, G.Q. Zhang, Viscoelastic characterization of low-dielectric-constant silk films using nano-indentation in combination with finite element modeling, J. Electron. Packag. 127 (2005) 267–285.

[31] P.L. Larsson, S. Carlsson, On microindentation of viscoelastic polymers, Polym. Test. 17 (1998) 49–75.
[32] K.L. Johnson, The correlation of indentation experiments, J. Mech. Phys. Solid 18 (1970) 115–128.
[33] Y. Lu, D.M. Shinozaki, Microindentation induced debonding of polymer thin films from rigid substrates, J. Mater. Sci. 37 (2002) 1283–1293.
[34] K.L. Johnson, Contact Mechanics, Cambridge University Press, 1985.
[35] A.E. Giannakopoulos, P.L. Larsson, R. Vestergaard, Analysis of vickers indentation, Int. J. Solids Struct. 31 (19) (1994) 2679–2708.
[36] P.L. Larsson, A.E. Giannakopoulos, E. Söderlund, D.J. Rowcliffe, R. Vestergaard, Analysis of Berkovich indentation, Int. J. Solids Struct. 33 (2) (1996) 221–248.
[37] H.G.H. Van Melick, O.F.J.T. Bressers, J.M.J. Den Toonder, L.E. Govaert, H.E.H. Meijer, A micro-indentation method for probing the craze-initiation stress in glassy polymers, Polymer 44 (8) (2003) 2481–2491.
[38] L. Anand, N.M. Ames, On modeling the micro-indentation response of an amorphous polymer, Int. J. Plast. 22 (6) (2006) 1123–1170.
[39] L.C.A. van Breemen, T.A.P. Engels, C.G.N. Pelletier, L.E. Govaert, J.M.J. den Toonder, Numerical simulation of flat-tip micro-indentation of glassy polymers: influence of loading speed and thermodynamic state, Philos. Mag. 89 (2009) 677–696.
[40] V. Jardret, H. Zahouani, J.L. Loubet, T.G. Mathia, Understanding and quantification of elastic and plastic deformation during a scratch test, Wear 218 (1) (1998) 8–14.
[41] B.L. Evans, The microhardness of injection moulded polystyrene and polyethylene, J. Mater. Sci. 24 (1) (1989) 173–182.
[42] B.H. Stuart, B.J. Briscoe, Scratch hardness studies of poly(ether ether ketone), Polymer 37 (17) (1996) 3819–3824.
[43] B.H. Stuart, Scratch friction studies of polycarbonate, Polym. Test. 16 (5) (1997) 517–522.
[44] E. Felder, J.L. Bucaille, Mechanical analysis of the scratching of metals and polymers with conical indenters at moderate and large strains, Tribol. Int. 39 (2) (2006) 70–87.
[45] J.L. Bucaille, E. Felder, G. Hochstetter, Experimental and three-dimensional finite element study of scratch test of polymers at large deformations, J. Tribol. 126 (2) (2004) 372–379.
[46] J.L. Bucaille, E. Felder, G. Hochstetter, Mechanical analysis of the scratch test on elastic perfectly plastic materials with the three-dimensional finite element modeling, Wear 249 (5-6) (2001) 422–432.
[47] J.H. Lee, G.H. Xu, H. Liang, Experimental and numerical analysis of friction and wear behavior of polycarbonate, Wear 250-251 (PART 2) (2001) 1541–1556.
[48] H. Pelletier, C. Gauthier, R. Schirrer, Experimental and finite-element analysis of scratches on amorphous polymeric surfaces, Mech. Ind. 9 (4) (2008) 261–271.
[49] H. Pelletier, C. Gauthier, R. Schirrer, Experimental and finite-element analysis of scratches on amorphous polymeric surfaces, Proc. Inst. Mech. Eng.: Part J. J. Eng. Tribol. 222 (3) (2008) 221–230.
[50] H. Pelletier, C. Gauthier, R. Schirrer, Strain and stress fields during scratch tests on amorphous polymers: influence of the local friction, Tribol. Lett. 32 (2) (2008) 109–116.
[51] H. Pelletier, A.L. Durier, C. Gauthier, R. Schirrer, Viscoelastic and elastic–plastic behaviors of amorphous polymeric surfaces during scratch, Tribol. Int. 41 (11) (2008) 975–984.
[52] H. Pelletier, C. Gauthier, R. Schirrer, Experimental measurement and numerical simulation of the plastic strain during indentation and scratch tests on polymeric surfaces, J. Mater. Res. 24 (3) (2009) 1184–1196.
[53] C. Gauthier, S. Lafaye, R. Schirrer, Elastic recovery of a scratch in a polymeric surface: experiments and analysis, Tribol. Int. 34 (7) (2001) 469–479.
[54] B.J. Briscoe, S.K. Sinha, Scratch resistance and localised damage characteristics of polymer surfaces – a review, Mater. wis. Werkstofftech. 34 (10-11) (2003) 989–1002.
[55] E.T.J. Klompen, T.A.P. Engels, L.E. Govaert, H.E.H. Meijer, Modeling of the postyield response of glassy polymers: influence of thermomechanical history, Macromolecules 38 (16) (2005) 6997–7008.
[56] L.C.A. van Breemen, E.T.J. Klompen, L.E. Govaert, H.E.H. Meijer, Extending the EGP constitutive model for polymer glasses to multiple relaxation times, J. Mech. Phys. Solids 59 (2011) 2191–2207.
[57] L.C.A. van Breemen, Contact Mechanics in Glassy Polymers, PhD thesis, Eindhoven University of Technology, 2009.
[58] T.A.P. Engels, L.E. Govaert, G.W.M. Peters, H.E.H. Meijer, Processing-induced properties in glassy polymers: application of structural relaxation to yield stress development, J. Polym. Sci. Part B 44 (8) (2006) 1212–1225.
[59] L.E. Govaert, T.A.P. Engels, E.T.J. Klompen, G.W.M. Peters, H.E.H. Meijer, Processing-induced properties in glassy polymers: development of the yield stress in PC, Int. Polym. Process. 20 (2) (2005) 170–177.
[60] C.G.N. Pelletier, E.C.A. Dekkers, L.E. Govaert, J.M.J. den Toonder, H.E.H. Meijer, The influence of indenter-surface misalignment on the results of instrumented indentation tests, Polym. Test. 26 (7) (2007) 949–959.
[61] MSC.Software. MSC.Marc Volume B: Element Library. MSC.Software GmbH, 2006.
[62] F.P. Bowden, A.J.W. Moore, D. Tabor, The ploughing and adhesion of sliding metals, J. Appl. Phys. 14 (2) (1943) 80–91.
[63] MSC.Software, MSC.Marc Volume A: Theory and User Information, MSC.Software GmbH, 2006.